Published in final edited form as:
AJR Am J Roentgenol. 2013 October ; 201(4): 795–800. doi:10.2214/AJR.12.9798.

Hepatocellular Carcinoma: Perfusion Quantification With Dynamic Contrast-Enhanced MRI

Bachir Taouli[1,2], **R. Scott Johnson**[2], **Cristina H. Hajdu**[3], **Marcel T. H. Oei**[2,4], **Miriam Merad**[5], **Herman Yee**[1,6], and **Henry Rusinek**[2]

[1]Department of Radiology, Body MRI, Translational and Molecular Imaging Institute, Mount Sinai School of Medicine, One Gustave Levy Pl, Box 1234, New York, NY 10029 [2]Department of Radiology, NYU Medical Center, New York, NY [3]Department of Pathology, NYU Medical Center, New York, NY [4]Department of Radiology, Radboud University Nijmegen Medical Centre, Nijmegen, The Netherlands [5]Department of Oncological Sciences, Mount Sinai School of Medicine, New York, NY

Abstract

OBJECTIVE—The objective of our study was to report our initial experience with dynamic contrast-enhanced MRI (DCE-MRI) for perfusion quantification of hepatocellular carcinoma (HCC) and surrounding liver.

SUBJECTS AND METHODS—DCE-MRI of the liver was prospectively performed on 31 patients with HCC (male-female ratio, 26:5; mean age, 61 years; age range, 41–83 years). A dynamic coronal 3D FLASH sequence was performed at 1.5 T before and after injection of gadolinium-based contrast agent with an average temporal resolution of 3.8 seconds. Regions of interest were drawn on the abdominal aorta, portal vein, liver parenchyma, and HCC lesions by two observers in consensus. Time-activity curves were analyzed using a dual-input single-compartment model. The following perfusion parameters were obtained: arterial flow, portal venous flow, arterial fraction, distribution volume, and mean transit time (MTT).

RESULTS—Thirty-three HCCs (mean size, 3.9 cm; range, 1.1–12.6 cm) were evaluated in 26 patients. When compared with liver parenchyma, HCC showed significantly higher arterial hepatic blood flow and arterial fraction ($p < 0.0001$) and significantly lower distribution volume and portal venous hepatic blood flow ($p < 0.0001$–0.023), with no difference in MTT. Untreated HCCs ($n = 16$) had a higher arterial fraction and lower portal venous hepatic blood flow value than chemoembolized HCCs ($n = 17$, $p < 0.04$).

CONCLUSION—DCE-MRI can be used to quantify perfusion metrics of HCC and liver parenchyma and to assess perfusion changes after HCC chemoembolization.

Address correspondence to B. Taouli (bachir.taouli@mountsinai.org).
[6]Deceased.

Keywords

chemoembolization; dynamic contrast-enhanced MRI; hepatocellular carcinoma; perfusion

Angiogenesis is critical for the growth and metastatic progression of hepatocellular carcinoma (HCC) [1–3] and involves different molecular pathways, including vascular endothelial growth factor [4–6]. HCC presents typically with an exclusive or near exclusive arterial supply, which prompts the use of transarterial chemoembolization (TACE) and systemic molecular targeted therapies [7, 8].

Dynamic contrast-enhanced MRI (DCE-MRI) enables quantification of the vascular characteristics of tissue and tumor [9–11]. DCE-MRI requires IV injection of a gadolinium-based contrast agent and uses high-temporal images that capture changes in MR signal intensity (SI) as a function of time. Tracer kinetic modeling based on DCE-MRI has been used to detect liver fibrosis and cirrhosis and to assess tumor angiogenesis [12–17]. Recent studies using perfusion CT [18–20] and DCE-MRI [16, 21–24] showed potential for quantifying perfusion of malignant liver lesions and for monitoring treatment response to antiangiogenic drugs in liver metastases. However, perfusion CT [18–20, 25] and DCE-MRI [16, 22, 26–28] data assessing HCC lesions and cirrhosis are limited. Some studies have shown differences in perfusion parameters between HCC tumors and background liver using perfusion CT [18–20] or a 2D gradient-recalled echo sequence for DCE-MRI [16].

With recent advances in MR hardware and software, it is now possible to cover the entire liver with adequate spatial and temporal resolution using a volumetric 3D sequence [15]. This sequence allows assessment of multiple lesions and of regional differences in liver parenchyma.

The purpose of our study was to report our early experience using 3D DCE-MRI with whole-liver coverage for the quantification of perfusion parameters of untreated HCC and treated HCC (TACE) compared with background cirrhotic liver.

Subjects and Methods

Patients

This prospective single-center study was HIPAA-compliant and was funded by a RSNA scholarship grant. Written informed consent for our institutional review board–approved study was obtained from all patients. Thirty-one patients with cirrhosis and HCC (male-female ratio, 26:5; mean age, 61 years; age range, 41–83 years) and with an estimated glomerular filtration rate of more than 60 mL/min/1.73 m^2 were enrolled in the study. The cause of cirrhosis was chronic hepatitis C (n = 20), chronic hepatitis B (n= 6), cryptogenic (n= 3), and unspecified (n = 2). HCC was diagnosed on liver explant (n = 8), liver resection specimen (n= 1), or liver biopsy (n= 4) or using updated American Association for the Study of Liver Diseases criteria (n= 18) [29].

Dynamic Contrast-Enhanced MRI

MRI was performed using one of three 1.5-T systems with torso phased-array coils (Magnetom Symphony, Sonata, or Avanto, Siemens Healthcare). DCE-MRI of the whole liver was performed using a volumetric interpolated spoiled gradient-recalled echo sequence (3D FLASH) in the coronal plane. Patients were asked to fast for 6 hours before the study. During scanning, the patients' arms were elevated to minimize aliasing artifacts. Three acquisitions were performed before contrast injection, and the first contrast-enhanced acquisition of the dynamic series started at the end of the injection of 10 mL of gadopentetate dimeglumine (Magnevist, Bayer HealthCare; $n = 26$) or gadobenate dimeglumine (MultiHance, Bracco Diagnostics; $n = 5$) followed by a 20-mL saline flush injected at 5 mL/s using an MR-compatible power injector (Spectris, Medrad). The following parameters were used: TR range/TE range, 1.7–3.2/0.8–1.2; flip angle, 12°; matrix, 156 × 192; 1 average; and FOV, 18 × 40 cm. A slab thickness of 18 cm, resulting in an interpolated slice thickness of 4 mm, was used. A parallel imaging technique (R factor 2 on the Symphony and Sonata systems and 3 on the Avanto system) using the generalized autocalibrating partial parallel acquisition (GRAPPA) was used. Forty coronal volumetric acquisitions were acquired for approximately 3–4 minutes (Fig. 1). The average temporal resolution was 3.8 seconds (range, 2.0–8.5 seconds, depending on the system). Patients were instructed to suspend respiration at end expiration during all 3D acquisitions, with the first breath-hold lasting approximately 25–30 seconds and subsequent shallow respiration. The rationale for using a 3D acquisition was to ensure that the entire liver was imaged. The rationale for imaging in the coronal plane was to minimize flow-related enhancement of the aorta.

The following routine MR sequences were performed for all examinations: T1 in-phase and out-of-phase, T2 fast spin-echo fat-suppressed, diffusion-weighted, and coronal T2 HASTE; in addition, a 3D T1-weighted sequence (VIBE) was performed before and after the initial injection of contrast material for DCE-MRI. An additional full dose of gadopentetate dimeglumine (0.1 mmol/kg, $n= 26$) or half dose of gadobenate dimeglumine (0.05 mmol/kg, $n= 5$) was injected for the routine contrast-enhanced study after completing the DCE-MRI acquisition.

Image Analysis

The images were transferred to a portable PC running Windows Vista (Microsoft). Software (Firevoxel) developed at our institution was used for analysis. HCC lesions were identified by two observers in consensus; observer 1 had 5 years of postgraduate experience and observer 2 was a medical student at the time of the study. The diagnosis was based on routine sequences including contrast-enhanced T1-weighted images and perfusion images. Regions of interest (ROIs) were manually drawn on the main portal vein at the level of the porta hepatis, proximal abdominal aorta at the level of the celiac axis, HCC, and background nontumoral liver tissue (away from HCC lesions) by observer 2 (average size of liver ROIs, 1 cm) to measure SI values. Given the small size of the hepatic artery, ROIs were instead drawn in the proximal abdominal aorta at the level of the celiac axis, which was used as a surrogate for the hepatic arterial blood supply. ROIs on the portal vein and HCC lesions were drawn for each time frame to correct for spatial misregistration due to respiratory

motion. For untreated lesions, ROIs were placed to fit lesion size; for treated lesions (i.e., after TACE), ROIs were placed on the enhancing component, which was identified on contrast-enhanced images. For lesions 2 cm or larger, data for two ROIs from two adjacent slices were averaged. The aorta and liver ROIs were drawn for a single time frame, were transferred to the remaining time frames, and were then manually corrected if necessary. Large vascular structures were avoided.

Perfusion Modeling

SI measurements were normalized by subtracting the SI value of the initial unenhanced image from the SI measurements of the subsequent enhanced images and then dividing the difference by the initial SI value. SI curves were then obtained from all ROI data. A linear relationship was assumed between SI and gadolinium concentration for the range of expected concentrations in the liver (0.0–0.5 mM/L) and blood (0–5 mM/L). Our conversion (*c*) was therefore based on the following approximation [30]:

$$c = k\,(S - S_0)/S_0,$$

where S_0 is unenhanced SI, S is contrast-enhanced SI, and k is the scaling constant (0.395 for liver and 0.201 for blood). These constants are based on a prior phantom and human calibration study [31]. The resulting time-concentration curves (Fig. 1) were fitted using a simple perfusion model that accounts for the dual blood supply of the liver through the hepatic artery and the portal vein [12, 13, 15]. Because the model considers the whole liver (capillaries, extravascular space, and cells) as a single functional compartment, determination of tissue blood fraction is not required. The model assumes a perfect extraction fraction of the contrast agent (instantaneous diffusion). This assumption is reasonable in the liver because endothelial fenestration is 50–200 nm, there is no basement membrane, and gadopentetate dimeglumine and gadobenate dimeglumine have has a small molecular diameter.

Based on computer simulations, the model yields precise parameters at clinical noise levels. The following parameters were obtained: arterial hepatic blood flow, portal venous hepatic blood flow, total hepatic blood flow, arterial fraction, distribution volume of gadolinium contrast material, and mean transit time (MTT) of gadolinium contrast material. The following parameters were calculated: distribution volume (as a percentage) of gadolinium contrast material through the liver compartment, mean transit time (in seconds) of gadolinium contrast material through the liver compartment, arterial hepatic blood flow (F_a, in mL/100 g/min), portal venous hepatic blood flow (in mL/100 g/min), total hepatic blood flow (F_t, in mL/100 g/min), and arterial fraction (as a percentage). The arterial fraction, or hepatic perfusion index, was calculated as follows:

$$100 \times F_a/F_t.$$

Statistical Analysis

The estimated perfusion parameters arterial hepatic blood flow, portal venous hepatic blood flow, total hepatic blood flow, arterial fraction, distribution volume, and MTT were compared between HCC and surrounding cirrhotic liver using a paired Wilcoxon test because the parameters did not follow a normal distribution. The estimated perfusion parameters of untreated HCCs were compared with those of treated HCCs after TACE using a Mann-Whitney test.

Results

Patients

Five patients with five treated HCCs were excluded because complete tumor necrosis was achieved after TACE and there was no contrast uptake, thus preventing any perfusion quantification. The final analysis included 33 HCCs (mean, 3.9 cm; range, 1.1–12.6 cm) in 26 cirrhotic patients. Twelve patients had untreated HCCs, and 11 had HCCs that were assessed after TACE, and three patients had HCCs that were assessed before and after TACE. The treated HCCs had a mean percentage necrosis estimated on subtracted contrast-enhanced images of 50% (range, 0–100%). In the 13 patients with histopathologic confirmation, HCCs were moderately differentiated in five patients and well differentiated in three patients; in the five remaining patients, this information could not be specified because complete tumor necrosis was achieved.

Dynamic Contrast-Enhanced MRI Findings

Comparison of estimated perfusion parameters in HCCs and liver parenchyma—When compared with liver parenchyma, HCC lesions showed significantly higher arterial hepatic blood flow and arterial fraction, lower distribution volume and portal venous hepatic blood flow, and no difference in MTT (Table 1 and Fig. 2). Compared with liver parenchyma, untreated HCCs had significantly higher arterial hepatic blood flow and arterial fraction, lower portal venous hepatic blood flow, and no difference in distribution volume and MTT (Figs. 1 and 2). Treated HCCs also had significantly higher arterial hepatic blood flow and arterial fraction, lower distribution volume, and no difference in portal venous hepatic blood flow and MTT compared with liver parenchyma (Figs. 2 and 3). There were no differences in perfusion parameters between moderately differentiated HCCs and well-differentiated HCCs; none of the assessed HCCs had poor differentiation.

Comparison of estimated perfusion parameters in untreated HCCs and treated HCCs—Untreated HCCs had a higher arterial fraction and lower portal venous hepatic blood flow than treated HCCs; no differences in the other parameters were detected (Table 1 and Figs. 2 and 3). Our series included three patients who underwent DCE-MRI before and after TACE using the same gadolinium contrast agent (Magnevist) (Table 2). When comparing perfusion parameters before and after TACE, there was a decrease in arterial fraction, arterial hepatic blood flow, and distribution volume and an increase in portal venous hepatic blood flow.

Discussion

Angiogenesis is critical for the growth and metastatic progression of HCC [1–3]. Investigators have suggested that HCC progresses from a small well-differentiated tumor with no developed arterial neovessels to a larger and moderately or poorly differentiated tumor with characteristic arterial hypervascularity [32]. The abundant, near exclusive arterial perfusion prompts the use of TACE and molecular targeted therapies [7, 8, 33]. Our results confirm that arterial flow is increased and portal venous flow is decreased in untreated HCCs compared with cirrhotic liver. Compared with untreated tumors, treated HCCs had lower arterial flow. Lost arterial supply is compensated for by an increase in portal flow, as shown in patients who had serial DCE-MRI scans before and after TACE. There was, however, a wide range of arterial and venous flow in untreated HCCs and treated HCCs, as shown in Figure 2. For HCCs naïve to therapy, this difference is likely because of variable amounts of angiogenesis. For treated HCCs, the wide range could result from the well known variability of tumor response to TACE. We thus believe that quantitative DCE-MRI provides a useful characterization of angiogenic activity and of HCC response to TACE. However, this should be verified in a prospective independent study.

Various perfusion models have been used to assess HCC and liver perfusion [18–20, 26–28]. Sahani et al. [18] used a distributed model to quantify perfusion on dynamic CT in 30 patients with advanced HCC. They found higher blood flow, blood volume, and permeability–surface area product in tumors compared with liver parenchyma, whereas MTT was lower in tumors. Using a model that separates arterial flow from portal venous flow, Ippolito et al. [20] found hepatic perfusion, blood volume, arterial perfusion, and hepatic perfusion index (equivalent to arterial fraction) to be significantly higher in HCC (n = 35) than in liver parenchyma. Dynamic CT has an advantage over DCE-MRI in that there is a direct linear relation between signal enhancement and iodine concentration. On the other hand, perfusion CT is limited by radiation exposure, which is especially problematic when follow-up studies are needed. Another advantage of DCE-MRI is its multiparametric imaging capability that allows DCE-MRI to be associated with diffusion-weighted MRI. Both dynamic contrast-enhanced CT [34, 35] and DCE-MRI can also be used for the detection of liver fibrosis and cirrhosis [12, 13, 15, 17, 36].

Few prior DCE-MRI studies have shown potential for quantifying perfusion and monitoring treatment response to systemic therapy in liver metastases [16, 23, 24] and HCC [16, 22, 26, 27] and to intraprocedural TACE [28]. Abdullah et al. [16] assessed perfusion parameters in 26 HCCs and 24 colorectal metastases using a deconvolution model. They found arterial hepatic blood flow, portal venous hepatic blood flow, total hepatic blood flow, and distribution volume to be significantly higher and MTT to be significantly lower in HCCs compared with metastases. Interestingly, they found no difference in arterial hepatic blood flow, and they also found that portal venous hepatic blood flow was slightly higher than arterial hepatic blood flow in HCCs in contradiction with our results. Recent studies have also shown that perfusion CT [25] and DCE-MRI [26, 27] have a potential role in monitoring HCC response to systemic therapy.

Our study has several limitations. First, our sample size is relatively small. Second, histopathologic confirmation of HCC was not available in all cases. Third, we used a different contrast agent with higher relaxivity (gadobenate dimeglumine) in a small subset of patients (n = 5). We do not believe that use of this agent affected perfusion quantification because we assumed linearity in all cases. Finally, our study used a simple one-compartment model based on simplifying assumptions, including an instantaneous mixing of the tracer between the vascular and the extravascular-extracellular space. Recently several more realistic physiologic models for liver perfusion were reported in the literature such as the two-compartmental model [37] and the distribution parameter model [38]. However, because of numerous DCE-MRI–related limitations, parameters derived from these models may lack sufficient precision for clinical application, and whether these models can be easily applied to liver tumors is not known.

In conclusion, these initial results confirm the presence of increased arterial flow and decreased portal venous flow in HCC compared with cirrhotic liver using DCE-MRI. In addition, there were significant differences in the degree of arterial versus portal venous blood flow in treated and untreated HCCs. These results suggest that DCE-MRI can be used as a noninvasive marker of HCC angiogenesis and may potentially be useful for characterizing cirrhotic nodules and for predicting and monitoring response to TACE and targeted antiangiogenic drugs currently in use in HCC.

Acknowledgments

This study received support from the Radiological Society of North America (RSNA scholarship grant RSCH 0710).

References

1. Nakashima T, Kojiro M. Pathologic characteristics of hepatocellular carcinoma. Semin Liver Dis. 1986; 6:259–266. [PubMed: 3022387]
2. Ng IO, Poon RT, Lee JM, Fan ST, Ng M, Tso WK. Microvessel density, vascular endothelial growth factor and its receptors Flt-1 and Flk-1/KDR in hepatocellular carcinoma. Am J Clin Pathol. 2001; 116:838–845. [PubMed: 11764072]
3. Dhar DK, Naora H, Yamanoi A, et al. Requisite role of VEGF receptors in angiogenesis of hepatocellular carcinoma: a comparison with angiopoietin/Tie pathway. Anticancer Res. 2002; 22:379–386. [PubMed: 12017318]
4. Connolly DT. Vascular permeability factor: a unique regulator of blood vessel function. J Cell Biochem. 1991; 47:219–223. [PubMed: 1791186]
5. Dvorak HF, Brown LF, Detmar M, Dvorak AM. Vascular permeability factor/vascular endothelial growth factor, microvascular hyperpermeability, and angiogenesis. Am J Pathol. 1995; 146:1029–1039. [PubMed: 7538264]
6. Ferrara N. Vascular endothelial growth factor. Eur J Cancer. 1996; 32:2413–2422. [PubMed: 9059329]
7. Bruix J, Sala M, Llovet JM. Chemoembolization for hepatocellular carcinoma. Gastroenterology. 2004; 127:S179–S188. [PubMed: 15508083]
8. Llovet JM, Ricci S, Mazzaferro V, et al. Sorafenib in advanced hepatocellular carcinoma. N Engl J Med. 2008; 359:378–390. [PubMed: 18650514]
9. Padhani AR. Dynamic contrast-enhanced MRI studies in human tumours. Br J Radiol. 1999; 72:427–431. [PubMed: 10505003]

10. Padhani AR. Dynamic contrast-enhanced MRI in clinical oncology: current status and future directions. J Magn Reson Imaging. 2002; 16:407–422. [PubMed: 12353256]
11. Parker GJ, Suckling J, Tanner SF, et al. Probing tumor microvascularity by measurement, analysis and display of contrast agent uptake kinetics. J Magn Reson Imaging. 1997; 7:564–574. [PubMed: 9170043]
12. Materne R, Smith AM, Peeters F, et al. Assessment of hepatic perfusion parameters with dynamic MRI. Magn Reson Med. 2002; 47:135–142. [PubMed: 11754452]
13. Annet L, Materne R, Danse E, Jamart J, Horsmans Y, Van Beers BE. Hepatic flow parameters measured with MR imaging and Doppler US: correlations with degree of cirrhosis and portal hypertension. Radiology. 2003; 229:409–414. [PubMed: 12970464]
14. Van Beers BE, Materne R, Annet L, et al. Capillarization of the sinusoids in liver fibrosis: noninvasive assessment with contrast-enhanced MRI in the rabbit. Magn Reson Med. 2003; 49:692–699. [PubMed: 12652540]
15. Hagiwara M, Rusinek H, Lee VS, et al. Advanced liver fibrosis: diagnosis with 3D whole-liver perfusion MR imaging—initial experience. Radiology. 2008; 246:926–934. [PubMed: 18195377]
16. Abdullah SS, Pialat JB, Wiart M, et al. Characterization of hepatocellular carcinoma and colorectal liver metastasis by means of perfusion MRI. J Magn Reson Imaging. 2008; 28:390–395. [PubMed: 18666145]
17. Patel J, Sigmund EE, Rusinek H, Oei M, Babb JS, Taouli B. Diagnosis of cirrhosis with intravoxel incoherent motion diffusion MRI and dynamic contrast-enhanced MRI alone and in combination: preliminary experience. J Magn Reson Imaging. 2010; 31:589–600. [PubMed: 20187201]
18. Sahani DV, Holalkere NS, Mueller PR, Zhu AX. Advanced hepatocellular carcinoma: CT perfusion of liver and tumor tissue—initial experience. Radiology. 2007; 243:736–743. [PubMed: 17517931]
19. Ippolito D, Sironi S, Pozzi M, et al. Perfusion computed tomographic assessment of early hepatocellular carcinoma in cirrhotic liver disease: initial observations. J Comput Assist Tomogr. 2008; 32:855–858. [PubMed: 19204443]
20. Ippolito D, Sironi S, Pozzi M, et al. Perfusion CT in cirrhotic patients with early stage hepatocellular carcinoma: assessment of tumor-related vascularization. Eur J Radiol. 2010; 73:148–152. [PubMed: 19054640]
21. Morgan B, Thomas AL, Drevs J, et al. Dynamic contrast-enhanced magnetic resonance imaging as a biomarker for the pharmacological response of PTK787/ZK 222584, an inhibitor of the vascular endothelial growth factor receptor tyrosine kinases, in patients with advanced colorectal cancer and liver metastases: results from two phase I studies. J Clin Oncol. 2003; 21:3955–3964. [PubMed: 14517187]
22. Wang J, Chen LT, Tsang YM, Liu TW, Shih TT. Dynamic contrast-enhanced MRI analysis of perfusion changes in advanced hepatocellular carcinoma treated with an antiangiogenic agent: a preliminary study. AJR. 2004; 183:713–719. [PubMed: 15333360]
23. Totman JJ, O'Gorman RL, Kane PA, Karani JB. Comparison of the hepatic perfusion index measured with gadolinium-enhanced volumetric MRI in controls and in patients with colorectal cancer. Br J Radiol. 2005; 78:105–109. [PubMed: 15681320]
24. Miyazaki K, Collins DJ, Walker-Samuel S, et al. Quantitative mapping of hepatic perfusion index using MR imaging: a potential reproducible tool for assessing tumour response to treatment with the antiangiogenic compound BIBF 1120, a potent triple angiokinase inhibitor. Eur Radiol. 2008; 18:1414–1421. [PubMed: 18351351]
25. Jiang T, Kambadakone A, Kulkarni NM, Zhu AX, Sahani DV. Monitoring response to antiangiogenic treatment and predicting outcomes in advanced hepatocellular carcinoma using image biomarkers, CT perfusion, tumor density, and tumor size (RECIST). Invest Radiol. 2012; 47:11–17. [PubMed: 21512396]
26. Jarnagin WR, Schwartz LH, Gultekin DH, et al. Regional chemotherapy for unresectable primary liver cancer: results of a phase II clinical trial and assessment of DCE-MRI as a biomarker of survival. Ann Oncol. 2009; 20:1589–1595. [PubMed: 19491285]
27. Yopp AC, Schwartz LH, Kemeny N, et al. Antiangiogenic therapy for primary liver cancer: correlation of changes in dynamic contrast-enhanced magnetic resonance imaging with tissue

hypoxia markers and clinical response. Ann Surg Oncol. 2011; 18:2192–2199. [PubMed: 21286939]

28. Wang D, Gaba RC, Jin B, et al. Intraprocedural transcatheter intra-arterial perfusion MRI as a predictor of tumor response to chemoembolization for hepatocellular carcinoma. Acad Radiol. 2011; 18:828–836. [PubMed: 21669349]
29. Bruix J, Sherman M. Management of hepatocellular carcinoma: an update. Hepatology. 2011; 53:1020–1022. [PubMed: 21374666]
30. Jones RA, Easley K, Little SB, Scherz H, Kirsch AJ, Grattan-Smith JD. Dynamic contrast-enhanced MR urography in the evaluation of pediatric hydronephrosis. Part 1. Functional assessment. AJR. 2005; 185:1598–1607. [PubMed: 16304021]
31. Bokacheva L, Rusinek H, Chen Q, et al. Quantitative determination of Gd-DTPA concentration in T1-weighted MR renography studies. Magn Reson Med. 2007; 57:1012–1018. [PubMed: 17534906]
32. Roskams T, Kojiro M. Pathology of early hepatocellular carcinoma: conventional and molecular diagnosis. Semin Liver Dis. 2010; 30:17–25. [PubMed: 20175030]
33. Abou-Alfa GK, Schwartz L, Ricci S, et al. Phase II study of sorafenib in patients with advanced hepatocellular carcinoma. J Clin Oncol. 2006; 24:4293–4300. [PubMed: 16908937]
34. Van Beers BE, Leconte I, Materne R, Smith AM, Jamart J, Horsmans Y. Hepatic perfusion parameters in chronic liver disease: dynamic CT measurements correlated with disease severity. AJR. 2001; 176:667–673. [PubMed: 11222202]
35. Ronot M, Asselah T, Paradis V, et al. Liver fibrosis in chronic hepatitis C virus infection: differentiating minimal from intermediate fibrosis with perfusion CT. Radiology. 2010; 256:135–142. [PubMed: 20574090]
36. Chen BB, Hsu CY, Yu CW, et al. Dynamic contrast-enhanced magnetic resonance imaging with Gd-EOB-DTPA for the evaluation of liver fibrosis in chronic hepatitis patients. Eur Radiol. 2012; 22:171–180. [PubMed: 21879400]
37. Larsson HB, Fritz-Hansen T, Rostrup E, Sondergaard L, Ring P, Henriksen O. Myocardial perfusion modeling using MRI. Magn Reson Med. 1996; 35:716–726. [PubMed: 8722823]
38. Koh TS, Thng CH, Lee PS, et al. Hepatic metastases: in vivo assessment of perfusion parameters at dynamic contrast-enhanced MR imaging with dual-input two-compartment tracer kinetics model. Radiology. 2008; 249:307–320. [PubMed: 18695207]

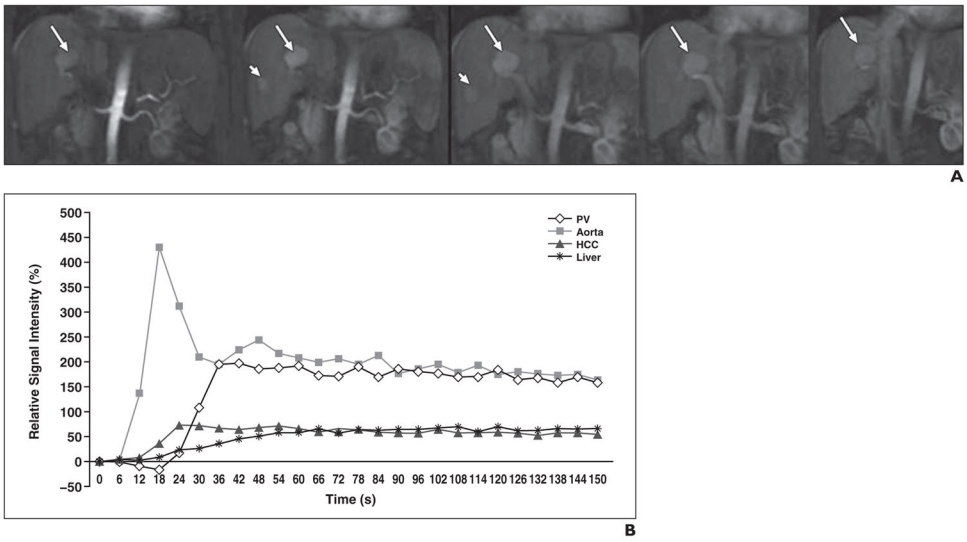

Fig. 1.

64-year-old man with liver cirrhosis secondary to chronic hepatitis C and two untreated hepatocellular carcinomas (HCCs).

A, Coronal dynamic contrast-enhanced MR images obtained with 3D FLASH sequence (TR/TE, 2.9/1.2; flip angle, 12°; voxel size, 2.6 × 2.1 × 4 mm; 1 average; parallel imaging factor, 3; temporal resolution, 6 seconds) covering entire liver before and after injection of 10 mL of gadopentetate dimeglumine. Two enhancing HCCs—one large lesion (*arrows*) and one small lesion (*arrowheads*)—are noted. Five selected time points from 40 measures are shown in chronologic order.

B, Corresponding time-activity curve shows early enhancement of largest HCC. Arterial fraction (HCC vs liver parenchyma, 81.1% vs 40.8%, respectively) and arterial hepatic blood flow (188.7 vs 64.8 mL/100 g/min) were both increased in HCC, whereas portal venous hepatic blood flow (44.1 vs 94.2 mL/100 g/min) and mean transit time (13.3 vs 19.8 seconds) were decreased in HCC compared with liver parenchyma. PV = portal vein.

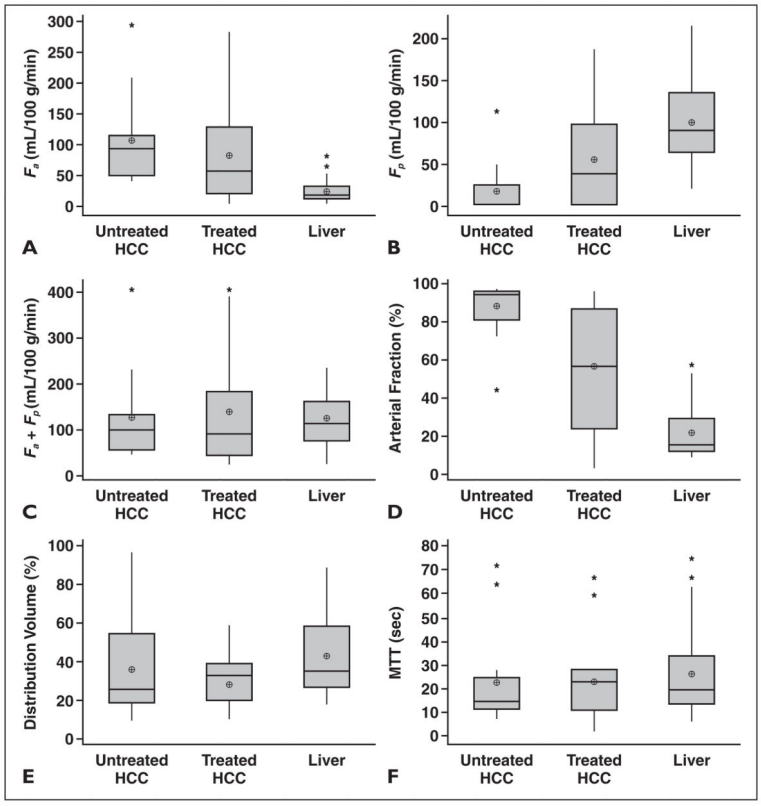

Fig. 2.

Box plot distributions of estimated perfusion parameters of 33 hepatocellular carcinoma (HCC) lesions, including untreated HCCs, treated HCCs, and liver parenchyma, in 26 patients measured with dynamic contrast-enhanced MRI. Top and bottom lines of boxes show 25–75th percentiles of data values. Lines in boxes show median values, and target signs in boxes show mean values; asterisks show outliers.

A, Arterial hepatic blood flow (F_a).

B, Portal venous hepatic blood flow (F_p).

C, Total hepatic blood flow ($F_a + F_p$).

D, Arterial fraction.

E, Distribution volume of gadolinium contrast material.

F, Mean transit time (MTT) of gadolinium contrast material.

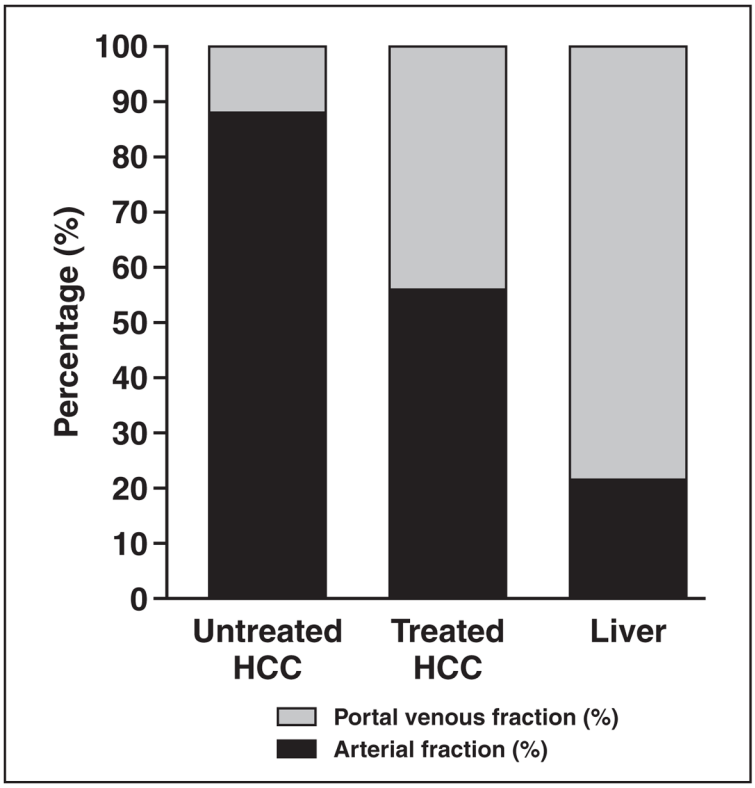

Fig. 3.

Bar graph shows distribution of arterial fraction and portal venous fraction (portal venous fraction = 100% – arterial fraction) of untreated hepatocellular carcinomas (HCCs), treated HCCs, and liver parenchyma measured using dynamic contrast-enhanced MRI. Arterial fraction is decreased in treated HCCs compared with untreated HCCs.

TABLE 1

Estimated Perfusion Parameters of 33 Hepatocellular Carcinoma (HCC) Lesions and of Surrounding Cirrhotic Liver in 26 Patients, Measured With Dynamic Contrast-Enhanced MRI

	Arterial Hepatic Blood Flow (mL/100 g/min)	Portal Venous Hepatic Blood Flow (mL/100 g/min)	Total Hepatic Blood Flow (mL/100 g/min)	Arterial Fraction (%)	Distribution Volume of Gadolinium Contrast Agent (%)	MTT (s)
All HCCs (*n* = 33)	95.1 ± 75.4	37.6 ± 48.5	132.8 ± 108.2	72.3 ± 29.4	33.4 ± 18.6	22.4 ± 18.6
Untreated HCCs (*n* = 16)	107.3 ± 72.1	18.8 ± 30.6	126.1 ± 96.2	88.3 ± 14.4	35.9 ± 23.2	22.3 ± 19.3
Treated HCCs (*n* = 17)	82.9 ± 79.1	56.5 ± 56.5	139.4 ± 122.1	56.3 ± 32.2	30.9 ± 12.7	22.5 ± 18.5
Liver (*n* = 26)	25.0 ± 17.6	99.8 ± 52.4	124.9 ± 55.8	21.5 ± 14.2	42.7 ± 19.9	25.7 ± 18.3
p						
All HCCs vs liver[a]	**< 0.0001**	**< 0.0001**	0.713	**< 0.0001**	**0.003**	0.261
Untreated HCCs vs liver[a]	**0.001**	**0.002**	0.222	**0.001**	0.074	0.5114
Treated HCCs vs liver[a]	**0.003**	0.079	0.490	**0.003**	**0.024**	0.346
Untreated HCCs vs treated HCCs[b]	0.254	**0.0381**	0.7875	**0.0032**	0.9504	0.9339

Note—All values except *p* values are expressed as mean ± SD. Significant *p* values are set in **boldface**. MTT = mean transit time.

[a] Paired Wilcoxon test.

[b] Mann-Whitney test.

AJR Am J Roentgenol. Author manuscript; available in PMC 2014 August 26.

TABLE 2

Estimated Perfusion Parameters Measured in Three Hepatocellular Carcinomas (HCCs) in Three Patients Before and After Transarterial Chemoembolization (TACE)

HCC	Arterial Hepatic Blood Flow (mL/100 g/min)	Portal Venous Hepatic Blood Flow (mL/100 g/min)	Total Hepatic Blood Flow (mL/100 g/min)	Arterial Fraction (%)	Distribution Volume of Gadolinium Contrast Agent (%)	MTT (s)	Tumor Necrosis (%)
Before TACE (mean ± SD)	88.6 ± 43.1	18.0 ± 25.9	106.6 ± 68.6	88.3 ± 12.3	27.8 ± 10.6	17.3 ± 4.0	16.6 ± 28.8
After TACE (mean ± SD)	41.8 ± 19.0	45.5 ± 64.9	87.3 ± 73.9	65.6 ± 32.2	17.9 ± 9.4	18.3 ± 11.1	90.0 ± 0
Mean difference (%)[a]	−47.1	12.7	−22.0	−23.1	−34.1	15.2	80.8 + 23.2

Note—There was a decrease in arterial hepatic blood flow, arterial fraction, and distribution volume and an increase in portal venous hepatic blood flow after TACE while tumors became necrotic. MTT = mean transit time.

[a]Calculated as follows: [(post-TACE value – pre-TACE value)/pre-TACE value] × 100%.